PERGAMON

International Journal of Heat and Mass Transfer 45 (2002) 3437–3446

International Journal of HEAT and MASS TRANSFER

www.elsevier.com/locate/ijhmt

A combined temperature scale for analyzing natural convection in rectangular enclosures with discrete wall heat sources

Qi-Hong Deng [a], Guang-Fa Tang [a,*], Yuguo Li [b]

[a] Department of Building Environment and Equipment, College of Civil Engineering, Hunan University, Changsha, Hunan 410082, China
[b] Department of Mechanical Engineering, The University of Hong Kong, Pokfulam Road, Hong Kong, China

Received 19 November 2001

Abstract

This paper presents a systematic numerical study on a two-dimensional, steady state and laminar natural convection in a rectangular enclosure with discrete heat sources on walls. A new combined temperature scale is suggested to non-dimensionalize the governing equations of natural convection induced by multiple temperature differences. It is valuable to simplify the coupled boundary conditions and to identify the relative strength of the heat source. The heat and fluid flow structures are fully examined using streamlines and heatlines. Numerical results demonstrate the suggested combined temperature scale being efficient to characterize the various roles of the heat sources and to provide an effective approach to analyze more realistic and complex natural convection problems.

1. Introduction

Natural convection in enclosures is an area of interest due to its wide applications and great importance in engineering, as comprehensively reviewed by Ostrach [1] and Bejian [2]. Considerable efforts in recent years have been exerted to deal with more complex and realistic boundary conditions occurring in practice, and can be summarized into four basic types as: the natural convection due to a uniformly heated wall, either prescribed by a temperature or a constant heat flux [3–5]; the natural convection induced by a local heat source [6–10]; the natural convection under multiple heat sources but with the same strength and type [11]; and the natural convection conjugated with inner heat-generating conducting body [12,13] or conjugated with the conducting walls [14,15].

All the studies mentioned above are based on a single temperature difference between the differentially heated walls. In spite of diversity in their physical aspects, they are of no numerical specialties and thus can be handled as usual. In practice, however, there are some cases that cannot be simplified and solved by the single temperature difference scale, such as natural convection induced by heat sources of different type and/or strength simultaneously, which occurring often in cooling electronic equipment and heating in rooms. The characteristics of fluid flow and heat transfer under the multiple temperature differences are more complicated and has a practical importance in thermal management and design.

The objective of the present work is to numerically analyze the natural convection under multiple temperature differences. A new combined temperature scale is suggested to deal with. The nature of the heat and fluid flow induced is investigated by means of streamlines and heatlines. Main attention is focused on the factors that influence the flow pattern and heat transfer, and also the interactions between the heat sources.

2. Mathematical formulation

Consider a two-dimensional natural convection in a fluid-filled cavity of side length L, as shown in Fig. 1. Two discrete heat sources are located at the upper part

* Corresponding author. Fax: +86-731-8821005.
E-mail address: gftang@mail.hunu.edu.cn (G.-F. Tang).

0017-9310/02/$ - see front matter
PII: S0017-9310(02)00060-1

Nomenclature

g	gravitational acceleration
H	dimensionless heatfunction
k	thermal conductivity of the fluid
L	characteristic length of the enclosure
l	length of the heat source
n	normal vector
N	the number of heat sources
Nu	Nusselt number
P	non-dimensional pressure
p	pressure
Pr	Prandtl number
q''	heat flux
Ra	Rayleigh number
T	temperature
u, v	velocity components
U, V	dimensionless velocities
x, y	Cartesian coordinates
X, Y	dimensionless coordinates

Greek symbols

α	thermal diffusivity of the fluid
β	coefficient of thermal expansion
ρ	density of the fluid
v	kinematic viscosity of the fluid
θ	dimensionless temperature
ψ	dimensionless streamfunction

Subscripts

c	cold wall
f	heat source flux
h	hot wall
max	maximum
t	isothermal heat source
i, j	the serial number of heat source

of the left side wall (length l_1) and left part of the bottom wall (length l_2), prescribed either by high surface temperature T_{h1} and/or T_{h2} or by heat flux q_1'' and/or q_2''. The right vertical side wall is maintained at a low temperature T_c ($T_c < T_h$), and the other parts of the enclosures are all insulated. The natural convection fluid flow and heat transfer is therefore set up by the two heat sources, and the heat transport path is also schematically shown in the figure. The natural convection under consideration can be classified accordingly into the following four cases as shown in Table 1: Case I with two higher temperature surfaces; Case II with left heat source of higher temperature surface and bottom of flux surface; Case III with left heat source of heat flux surface and bottom isothermal surface; and Case IV with two heat flux surfaces.

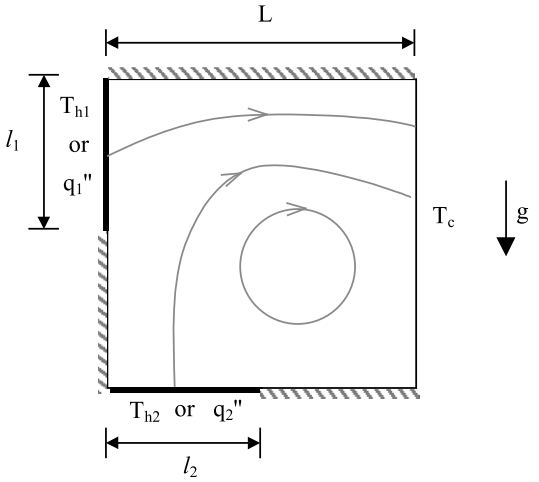

Fig. 1. Natural convection in square enclosures with two discrete heat sources on walls (the curves represent the energy/heat transport path).

2.1. Governing equations

The natural convection flows are considered, here, to be steady and laminar. The Boussinesq approximation is employed to account for the thermal buoyancy effects. Then, the governing equations in dimensionless form are as follows:

Continuity equation

$$\frac{\partial U}{\partial X}+\frac{\partial V}{\partial Y}=0. \tag{1}$$

Momentum equation

$$\frac{\partial}{\partial X}(UU)+\frac{\partial}{\partial Y}(VU)=-\frac{\partial P}{\partial X}+Pr\nabla^2 U, \tag{2}$$

$$\frac{\partial}{\partial X}(UV)+\frac{\partial}{\partial Y}(VV)=-\frac{\partial P}{\partial Y}+Pr\nabla^2 V+RaPr\theta. \tag{3}$$

Table 1
Natural convection with different type of heat sources

Cases	Heat source 1	Heat source 2
Case I	T_{h1}	T_{h2}
Case II	T_{h1}	q_2''
Case III	q_1''	T_{h2}
Case IV	q_1''	q_2''

Energy equation

$$\frac{\partial}{\partial X}(U\theta)+\frac{\partial}{\partial Y}(V\theta)=\nabla^2\theta. \tag{4}$$

The governing equations are non-dimensionalized using the following reference scales: Length scale: L; Velocity scale: α/L; Temperature scale: ΔT (to be defined later).

The corresponding dimensionless variables are defined as

$$(X,Y)=\frac{(x,y)}{L},\quad (U,V)=\frac{(u,v)}{\alpha/L},$$
$$P=\frac{p}{\rho(\alpha/L)^2},\quad \theta=\frac{T-T_c}{\Delta T} \tag{5}$$

and the dimensionless parameters are

$$Pr=\nu/\alpha,\quad Ra=g\beta\Delta TL^3/\nu\alpha. \tag{6}$$

Accordingly, the thermal boundary conditions (BCs) of the cold and adiabatic walls are respectively $\theta=0$ and $\partial\theta/\partial n=0$. No-slip condition is applied to the velocity BCs for all the enclosed walls.

The local Nusselt number for the isothermal surface is defined as

$$Nu=-\frac{\partial\theta}{\partial n}. \tag{7}$$

The average Nusselt number ($\overline{Nu}$) is obtained by integrating Eq. (7) along the surface.

2.2. Combined temperature scale

It would need to establish an approach for determining the effects of discrete heat sources and their interactions. To this end, one should define a suitable temperature scale, ΔT. A new combined temperature scale is proposed as follows:

$$\begin{aligned}&\text{For Case I}: \Delta T=(T_{h1}-T_c)+(T_{h2}-T_c);\\ &\text{For Case II}: \Delta T=(T_{h1}-T_c)+q_2''L/k;\\ &\text{For Case III}: \Delta T=q_1''L/k+(T_{h2}-T_c);\\ &\text{For Case IV}: \Delta T=q_1''L/k+q_2''L/k.\end{aligned} \tag{8}$$

It is interesting to find that a close relation exists as:

$$\begin{aligned}&\text{For Case I}: \theta_1+\theta_2=1;\\ &\text{For Case II}: \theta_1+\left(-\frac{\partial\theta}{\partial n}\right)_2=1;\\ &\text{For Case III}: \left(-\frac{\partial\theta}{\partial n}\right)_1+\theta_2=1;\\ &\text{For Case IV}: \left(-\frac{\partial\theta}{\partial n}\right)_1+\left(-\frac{\partial\theta}{\partial n}\right)_2=1,\end{aligned} \tag{9}$$

which written in general form as

$$\theta_{BC1}+\theta_{BC2}=1. \tag{10}$$

This indicates that the BCs for the two discrete heat sources are conjugated.

It is important to note that this approach is general to describe the natural convection induced by multiple discrete heat sources. For an enclosure with (N_t+1) boundaries with constant temperature and N_f boundaries with constant heat flux, the above combined temperature scale can be easily extended as

$$\Delta T=\sum_{i=1}^{N_t}(T_{hi}-T_c)+\sum_{j=1}^{N_f}\left(\frac{q_j''L}{k}\right). \tag{11}$$

The relation between the boundary conditions of the heat sources will be

$$\sum_{i=1}^{N_t}\theta_i+\sum_{j=1}^{N_f}\left(-\frac{\partial\theta}{\partial n}\right)_j=1. \tag{12}$$

For simpler problems as those analyzed in this paper, the combined temperature scale is also useful to show the relative strength of various wall heat sources.

2.3. Streamfunction and heatfunction

The streamline and heatline as detailed in [16,17], is adapted here to study the mass and energy/heat transport principle. According to the continuity and energy equation, the corresponding nondimensional streamfunction, ψ, and heatfunction, H, are, respectively, as:

$$\frac{\partial\psi}{\partial Y}=U,\quad -\frac{\partial\psi}{\partial X}=V, \tag{13}$$

$$\frac{\partial H}{\partial Y}=U\theta-\frac{\partial\theta}{\partial X},\quad -\frac{\partial H}{\partial X}=V\theta-\frac{\partial\theta}{\partial Y}. \tag{14}$$

The two functions could be evaluated once the primitive governing variables (U, V and θ) being solved, and subsequently the streamlines and heatlines can be plotted by contours of these functions.

3. Numerical results and discussion

The governing Eqs. (1)–(4) are discretized by a finite volume method and the coupling between velocity and pressure is solved by SIMPLE algorithm [18]. The third-order deferred correction QUICK scheme [19] and the second-order central difference are, respectively, implemented for the convection and diffusion terms. The resulting set of discretized equations for each variable are solved by a line-by-line procedure, combining the tri-diagonal matrix algorithm (TDMA) and the successive over-relaxation iteration (SOR). The convergence criterion is that the maximal residual of all the governing equations is less than 10^{-6}.

Non-uniform staggered grid system is employed in the present study with denser grids clustering near the

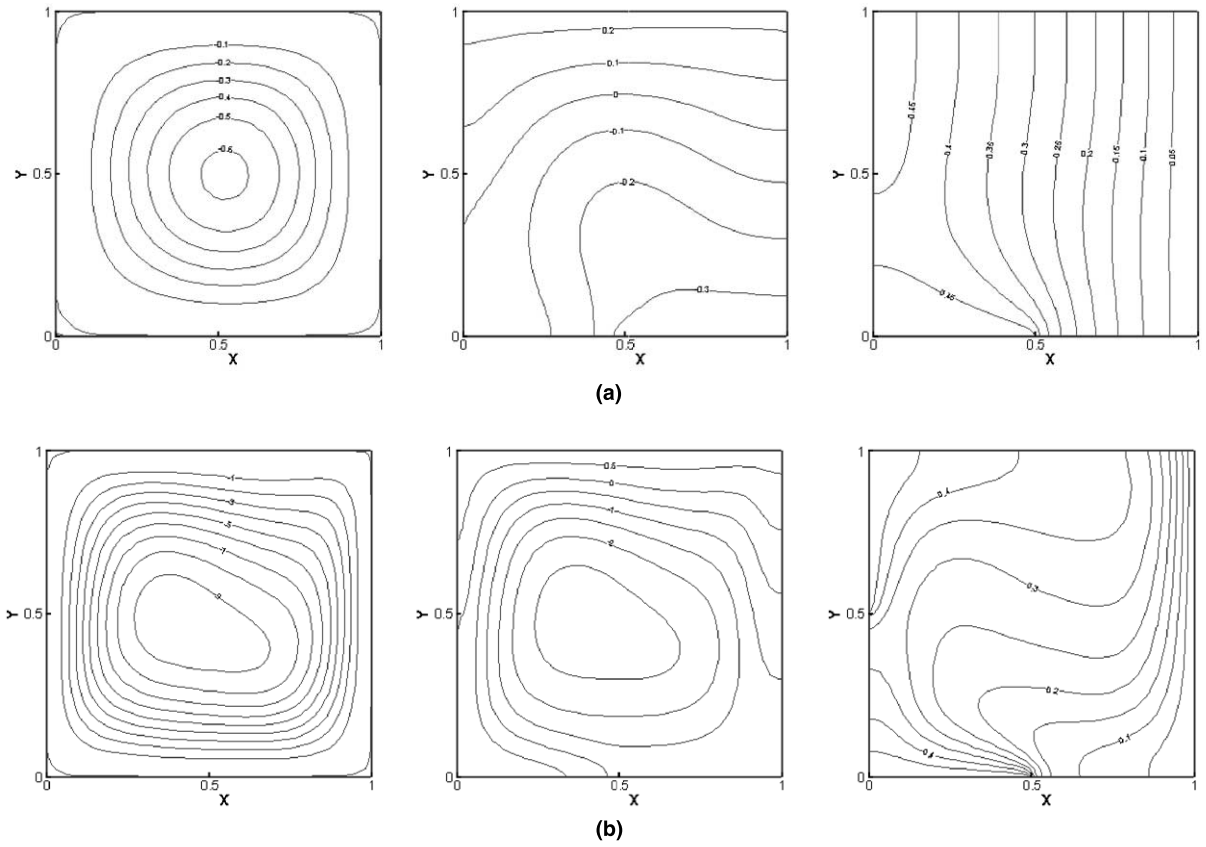

Fig. 2. Effects of the Ra for Case I with $\theta_{BC1} = \theta_{BC2} = 0.5$ and $l_1/L = l_2/L = 0.5$: (a) $Ra = 10^3$; (b) $Ra = 10^5$. The contour lines are respectively streamlines (left), heatlines (center) and isotherms (right).

enclosed walls so as to resolve the boundary layer properly. It was found that the grid 46×46 is sufficiently fine to ensure a grid independent solution. Accuracy of the numerical procedure is first validated by the comparison between the predicted results with the benchmark solutions of de Vahl Davis [20] for the natural convection in an air-filled square cavity. As shown in Table 2, good agreements were achieved for both the maximal streamfunction and the average Nusselt number in a broad range of Rayleigh number $Ra = 10^3$–10^6.

We will analyze the effect of Rayleigh number, and the size and strength of the heat source for each case of natural convection as listed in Table 1.

3.1. Case I – Dirichlet boundary conditions

3.1.1. Effects of Rayleigh number (Ra)

With $\theta_{BC1} = \theta_{BC2} = 0.5$ and $l_1/L = l_2/L = 0.5$, Fig. 2 shows the streamlines, heatlines and isotherms for $Ra = 10^3$ and 10^5, respectively. As shown in Fig. 2(a), the convection is very weak, when Rayleigh number is low as $Ra = 10^3$, and the flow pattern consists of unicellular streamlines with $|\psi|_{max} \approx 0.6$. Accordingly, the heat is mainly transported by conduction. Note that, as pointed out by Deng and Tang [16,17], the value difference between the heatlines across the cold wall is equal to the average Nusselt number of the surface, i.e. $\overline{Nu}_c = \Delta H_c \approx 0.5$, which implies that the heat transfer is very weak because of the low conductivity of air.

It is to be expected that, as the Rayleigh number increases, the convection may become stronger and the convective heat transfer becomes more important. The

Table 2
Comparisons between the predicted results and the benchmark resolutions of de Vahl Davis [20] for natural convection in air filled square cavity ($Pr = 0.71$)

Ra	Present		Benchmark	
	$\lvert\psi\rvert_{max}$	$\overline{Nu}$	$\lvert\psi\rvert_{max}$	$\overline{Nu}$
10^3	1.17	1.118	–	1.118
10^4	5.04	2.254	–	2.243
10^5	9.50	4.557	9.612	4.519
10^6	16.32	8.826	16.750	8.800

results for $Ra = 10^5$, are shown in Fig. 2(b), with $|\psi|_{max} \approx 9$, which indicate that the role of convection becomes prevailing. The heat transfer is therefore enhanced substantially with $\overline{Nu}_c = \Delta H_c \approx 2.0$. This demonstrates that the heat is mostly conveyed by the dominating convection.

3.1.2. Effects of thermal strength of heat sources (θ_{BC1} and θ_{BC2})

We compared the results for $Ra = 10^5$ and $l_1/L = l_2/L = 0.5$, shown in Fig. 3, with that from Fig. 2(b). Fig. 3(a) shows the results for $\theta_{BC1} = 0.3$ and $\theta_{BC2} = 1 - \theta_{BC1} = 0.7$, in which the surface temperature is lower on heat source 1 than that on heat source 2, the thermal strength of source 1 is weaker than that of source 2. For $\theta_{BC1} = \theta_{BC2} = 0.5$ in Fig. 2(b), the strength of two heat sources is identical, while Fig. 3(b) illustrates the results of $\theta_{BC1} = 0.7$ and $\theta_{BC2} = 0.3$, where the heat source 1 is obviously stronger than source 2. Thus, increasing the flux strength of heat source 1, or decreasing the flux strength of heat source 2, would substantially degrade the magnitude of convection, $|\psi|_{max}$ monotonously reduced from about 12 to 7 as the thermal strength of heat source 1 (θ_{BC1}) increased from 0.3 to 0.7. We can see that with increasing the flux strength of heat source 1, the thermal boundary layer along the surface was developed gradually. For the temperature gradient formed in the thermal boundary layer is reverse to the upward flow, the thermal layer has a stabilizing effect on the natural convection, i.e. decreasing the power of convection, as pointed out by Ostrach et al. [21].

When heat source 1 is weaker than 2 (see Fig. 3(a)), no heat will be transferred from heat source 1 to the opposite cold side wall, there is some amount of heat, being transferred from the higher temperature surface of heat source 2 to the relatively low temperature surface of heat source 1. When the strengths of the two heat sources are equal to each other (see Fig. 2(b)), somewhat more heat is transferred from the floor source, which indicated the role of heat source on the floor would be greater than that of heat source on the side wall. When the surface temperature of heat source 1 is much higher than heat source 2 (see Fig. 3(b)), it is expected that more heatlines come from the former than the latter for the weakened convection.

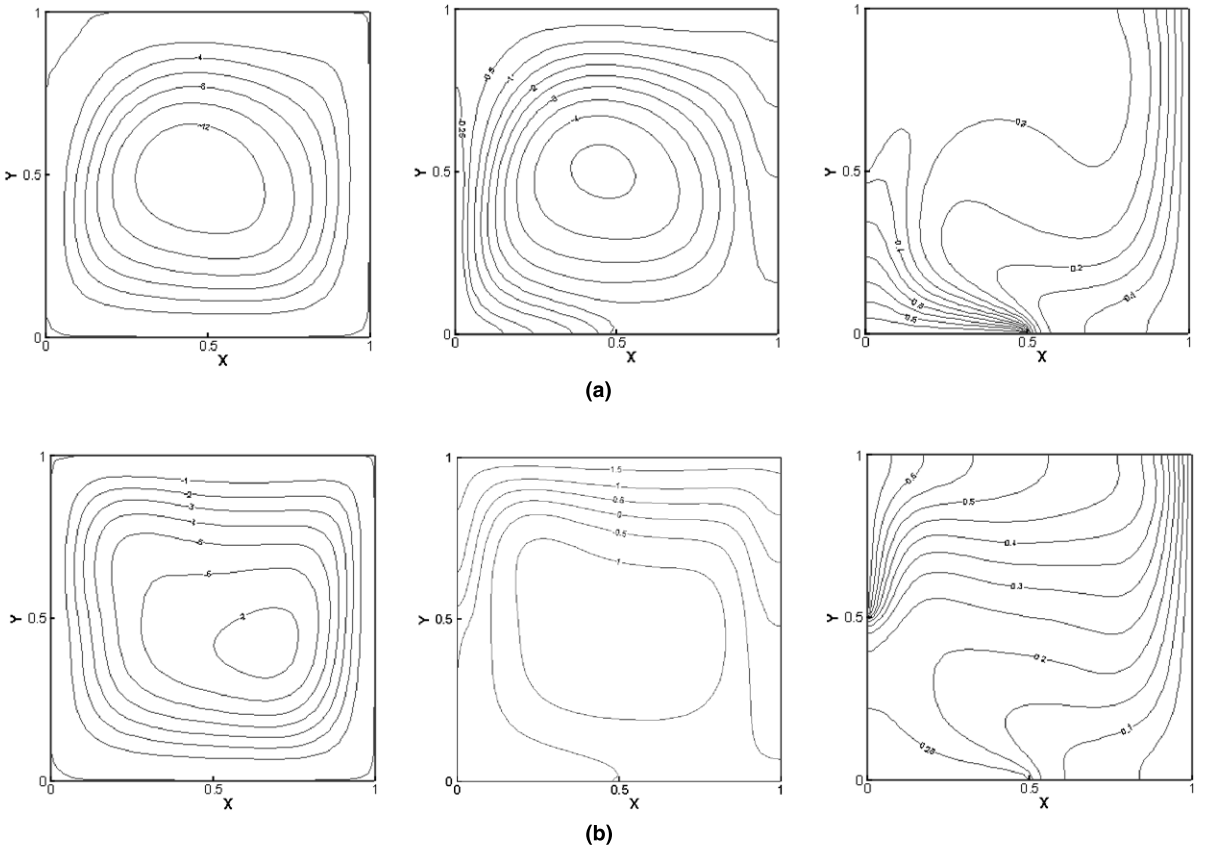

Fig. 3. Effects of surface temperature of heat sources for Case I with $Ra = 10^5$ and $l_1/L = l_2/L = 0.5$ by streamlines, heatlines and isotherms: (a) $\theta_{BC1} = 0.3$, $\theta_{BC2} = 0.7$; (b) $\theta_{BC1} = 0.7$; $\theta_{BC2} = 0.3$.

3.1.3. Effects of size of heat sources (l_1/L and l_2/L)

Table 3 lists the results obtained for different l_1/L, with $Ra = 10^5$, $\theta_{BC1} = \theta_{BC2} = 0.5$ and $l_2/L = 0.5$. From the changing trend of the streamfunction $|\psi|_{max}$, one can see that when $l_1/L \leqslant 0.5$, increasing the size of heat source on the left side wall would decrease the natural convection, or increase convection when $l_1/L \geqslant 0.5$. Therefore, for $l_1/L = 0.5$, the convection decreased to the lowest value, $|\psi|_{max} = 9.70$. Seen from Table 3, increasing the size of heat source, l_1/L, would enhance the convective heat transfer on its surface, and at the meantime weaken the heat transfer occurring on the other heat source, but the former is always larger than the latter, so the overall heat transfer of the system is improved.

The size effect of the bottom heat source, l_2/L, is shown in Table 4 with $Ra = 10^5, \theta_{BC1} = \theta_{BC2} = 0.5$ and $l_1/L = 0.5$. It is clear that the natural convection monotonously increases with the length of heat source 2. This is different from the size effect of heat source 1, for the increasing size of heat source on the floor would increase the thermal instability that contributes to the

Table 3
Effects of the l_1/L for $Ra = 10^5$ with $\theta_{BC1} = \theta_{BC2} = 0.5$ and $l_2/L = 0.5$

l_1/L	$\lvert\psi\rvert_{max}$	$\overline{Nu}_1$	$\overline{Nu}_2$	$\overline{Nu}_c$
0.0	11.60	–	1.355	1.353
0.2	10.50	0.299	1.306	1.603
0.4	9.84	0.555	1.269	1.822
0.5	9.70	0.674	1.251	1.924
0.6	9.72	0.777	1.235	2.010
0.8	10.06	0.907	1.214	2.120
1.0	10.16	0.958	1.181	2.137

Table 4
Effects of the l_2/L for $Ra = 10^5$ with $\theta_{BC1} = \theta_{BC2} = 0.5$ and $l_1/L = 0.5$

l_2/L	$\lvert\psi\rvert_{max}$	$\overline{Nu}_1$	$\overline{Nu}_2$	$\overline{Nu}_c$
0.2	7.385	0.935	0.637	1.570
0.4	8.866	0.754	1.061	1.812
0.6	10.555	0.597	1.442	2.036
0.8	12.22	0.459	1.808	2.265

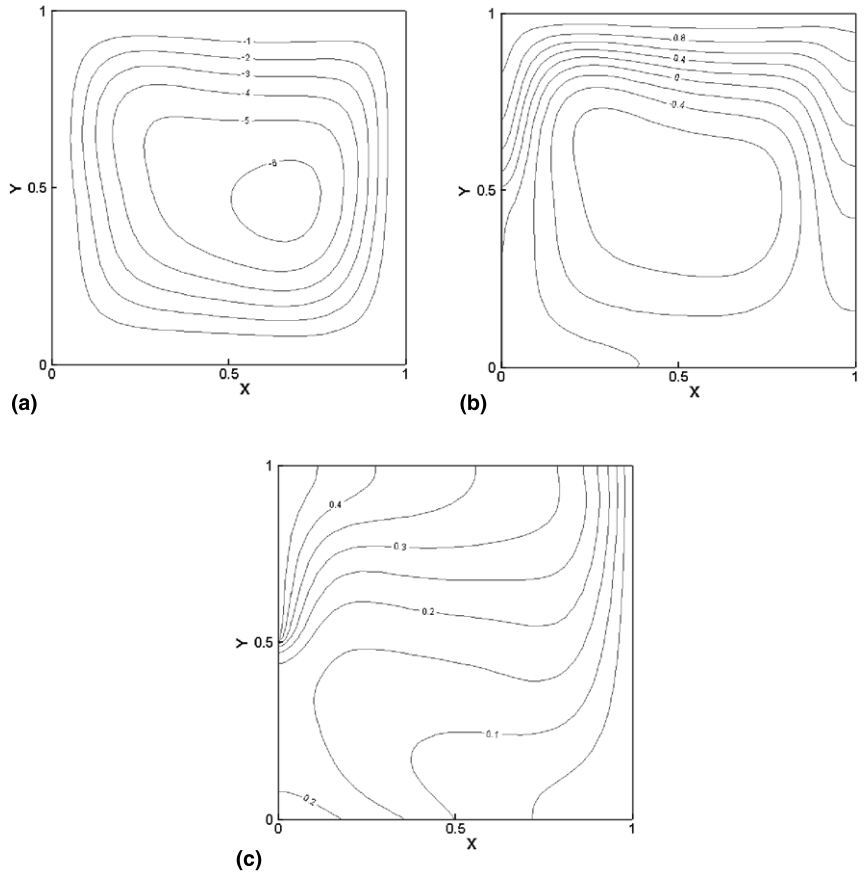

Fig. 4. Results for $Ra = 10^5$ Case II with $\theta_{BC1} = \theta_{BC2} = 0.5$ and $l_1/L = l_2/L = 0.5$ by streamlines (a), heatlines (b) and isotherms (c).

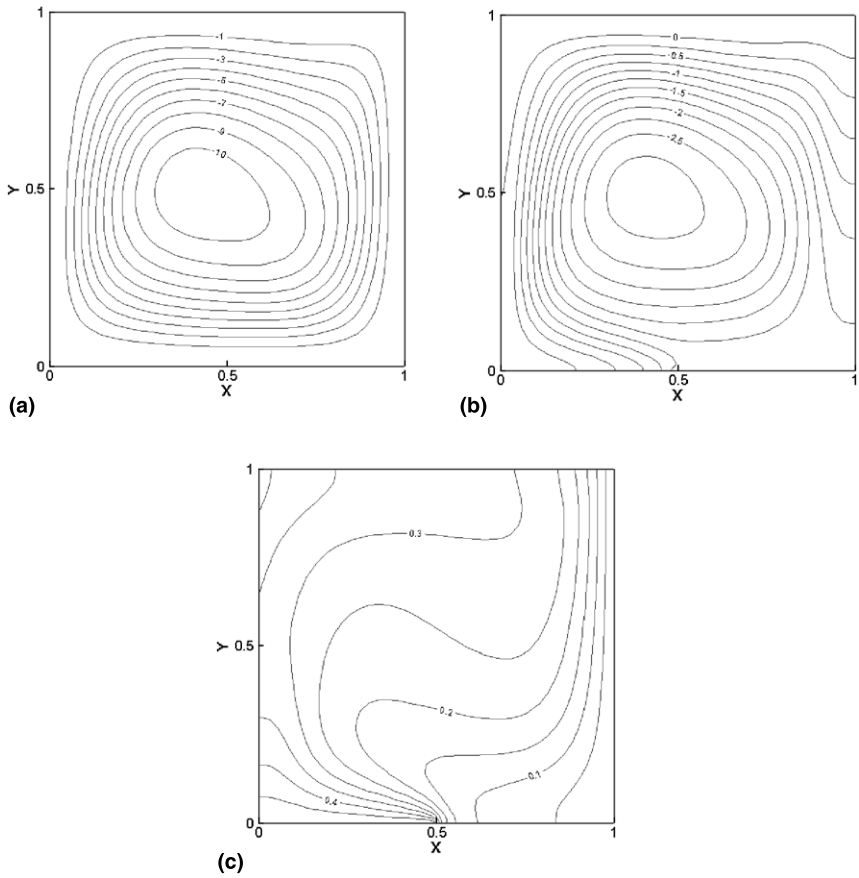

Fig. 5. Results for $Ra = 10^5$ Case III with $\theta_{BC1} = \theta_{BC2} = 0.5$ and $l_1/L = l_2/L = 0.5$ by (a) streamlines, (b) heatlines and (c) isotherms.

growing convection. The size effect of heat source is more vigorous on the floor than on the side wall for the role of the former is stronger than that of the latter as discussed before. The same trend of thermal behavior as the left heat source is also found.

3.2. Cases II–IV – Combined Dirichlet and Neumann BCs, and Neumann BCs

Having the background of Case I, we can briefly give the results for the other cases. Results of Cases II–IV for $Ra = 10^5$, $\theta_{BC1} = \theta_{BC2} = 0.5$, and $l_1/L = l_2/L = 0.5$ are respectively shown in Figs. 4–6 about the streamlines, the heatlines and the isotherms. The heat sources of Cases II and III are both combination of an isothermal surface and a flux surface. The overall heat transfer of the system was dominated by the isothermal heat source, and the effect of the flux surface is not as strong as that of the isothermal heat source. For Case II, the convective flow was suppressed by the stabilizing thermal boundary layer developed near the upper left isothermal surface (see isotherms in Fig. 4), so the convection was degraded with $|\psi|_{max} = 6$, while Case III, the convection was enhanced due to the instability of thermal boundary layer near the floor source, as seen $|\psi|_{max} = 10$ in Fig. 5. With two heat sources being both of flux surfaces, the similar behavior occurs on the heat source surfaces (Fig. 6) for Case IV. However, the heat transfer in Case IV is very low, as indicated by heatlines $\overline{Nu}_c = \Delta H_c \approx 0.5$ as compared to $\overline{Nu}_c = \Delta H_c \approx 1.2$ in the other two cases.

3.3. Comparisons of results with different boundary conditions

We compared the variations of the characteristics of fluid flow and heat transfer due to Rayleigh number and heat source properties (size, type, strength) of heat sources for the four cases, as respectively plotted in Figs. 7–10 in terms of the variations of the maximal stream-function and average Nusselt number. It is found from Fig. 7 that, for all the four cases, the convection increases as Ra increased. The tendency is more distinct for Cases I and III where the heat sources on floor are both isothermal higher temperature surface. This can be

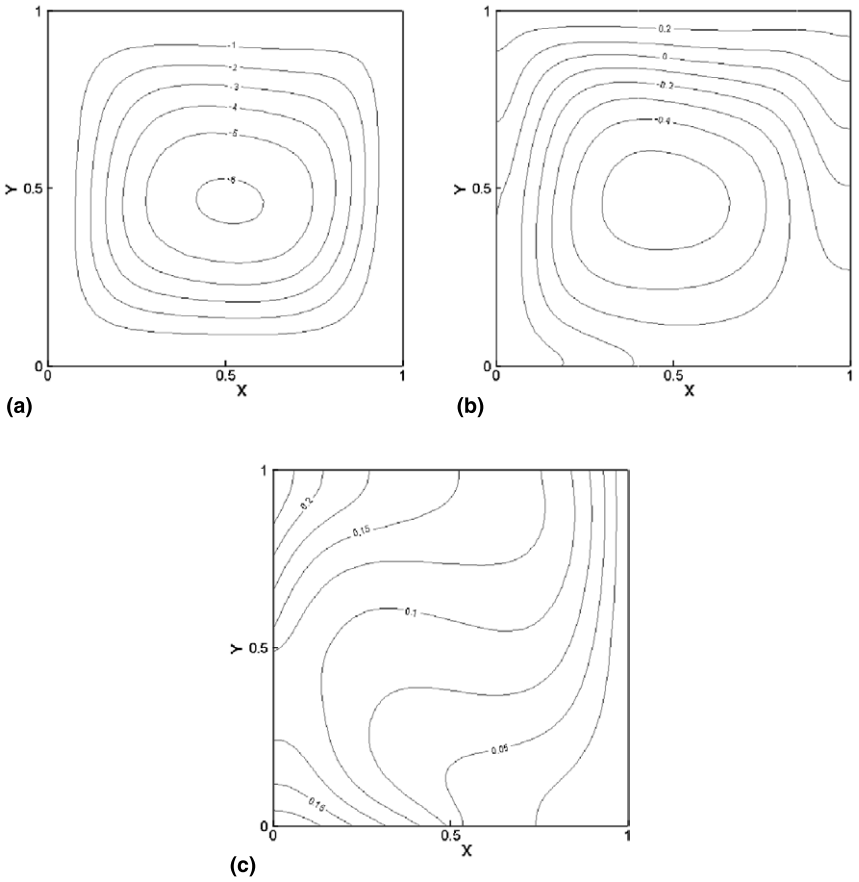

Fig. 6. Results for $Ra = 10^5$ Case IV with $\theta_{BC1} = \theta_{BC2} = 0.5$ and $l_1/L = l_2/L = 0.5$ by (a) streamlines, (b) heatlines and (c) isotherms.

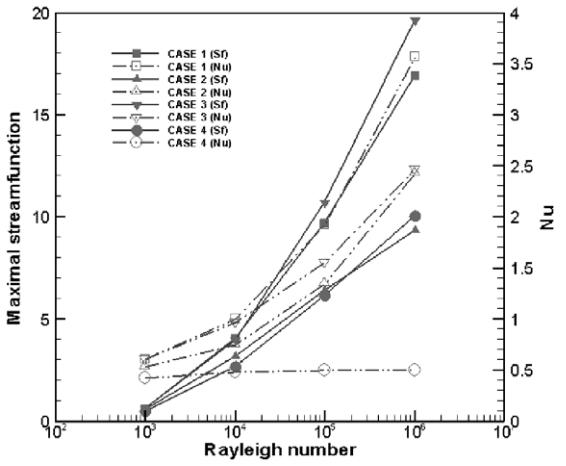

Fig. 7. Effects of Rayleigh number on the convection (maximal streamfunction) and overall heat transfer ($\overline{Nu}$) for all Cases I–IV.

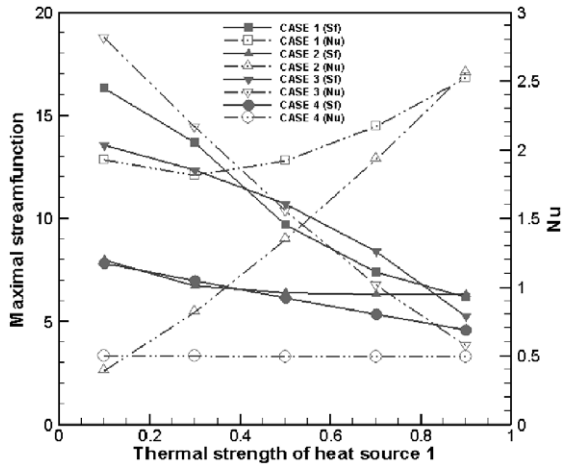

Fig. 8. Effects of thermal strength of heat source 1 on the convection (maximal streamfunction) and overall heat transfer ($\overline{Nu}$) for all Cases I–IV.

explained as the convection being mainly determined by the heat source on the floor and the isothermal surface being much stronger than the flux surface. The average Nusselt number, $\overline{Nu}$, increases with increasing Ra fastest

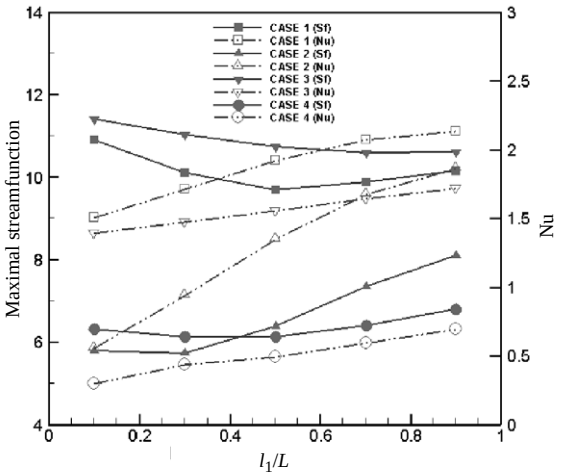

Fig. 9. Effects of length of heat source 1 on the convection (maximal streamfunction) and overall heat transfer ($\overline{Nu}$) for all Cases I–IV.

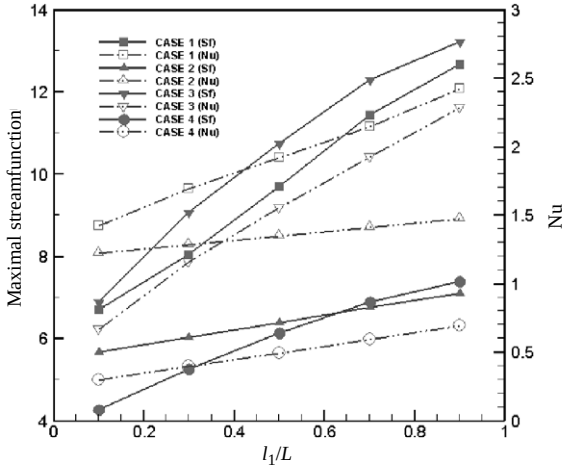

Fig. 10. Effects of length of heat source 2 on the convection (maximal streamfunction) and overall heat transfer ($\overline{Nu}$) for all Cases I–IV.

for Case I, then for Cases II and III, and slowest for Case IV where it is almost kept invariant. Notice that the heat transfer is mainly dominated by the isothermal heat source; there are two isothermal surfaces in Case I, one isothermal surface in the Cases II or III, and no isothermal surface in Case IV.

Fig. 8 shows the maximal streamfunction and average Nusselt number as functions of the thermal strength of heat source 1. For all the four cases, the convection decreases with strenthening the heat source 1, the change is more notable for Cases I and III. The overall heat transfer for Cases II and III is mainly affected by the isothermal heat source, i.e. the heat transfer is basically determined by the heat source 1 in Case II, or by the heat source 2 on the floor in Case III, and small changes for Cases I and IV.

The effects of heat source size on the characteristics of the convection and heat transfer are presented in Figs. 9 and 10. The trends of variation for Cases I and IV are similar, but the former being more obvious. The hyperbolic curve reveals that the convection reaches the lowest at the middle size of heat source 1, as detailed before. For Case II, the isothermal heat source 1 is the main impetus of convection, and thus the convection increases with l_1/L. For Case III, however, the convection decreases as the size of heat source decreases. The overall heat transfer monotonously increases with increasing l_1/L source 1 for all cases, but the trends for Cases I and II are more evident because their heat sources 1 are isothermal surfaces.

From Fig. 10, increasing length of heat source 2, l_2/L, would increase convection for all cases, but more significantly for Cases I and III. It is obvious that the size effect of heat source on floor is much stronger than that of the heat source on the side wall, as shown in Fig. 9. The same trend is also observed for the variations of the average Nusselt number.

In short, we can observe from Figs. 7–10 that, the natural convection for Cases I and III are sensitive to the boundary conditions (including *Ra*, the size, and strength of the heat source). The convection is mainly determined by the isothermal heat source on the floor.

4. Conclusion

A two-dimensional, laminar natural convection induced by multiple wall heat sources has been numerically studied. A combined temperature scale was suggested. The method proposed is general and efficient to define the complex boundary conditions, and also convenient to evaluate the interactions between the heat sources on the overall heat and fluid flow structures.

For the natural convection considered in this paper, some conclusions can be drawn as below: 1. The role of isothermal heat source is generally much stronger than the flux of heat source. 2. The heat source on the floor increases the thermal instability and thus acts a proportional effect on convection, while the heat source on the side wall increases the thermal stability and thus acts a reverse effect on convection. 3. The heat source on the floor can be more active than that on the side wall.

Acknowledgements

The authors would like to thank Prof. Xianting Li of Tsinghua University for his useful suggestions and discussions.

References

[1] S. Ostrach, Natural convection in enclosures, ASME J. Heat Transfer 110 (1998) 1175–1190.

[2] A. Bejan, Convection Heat Transfer, New York, Wiley, 1982.

[3] M.M. Ganzarolli, L.F. Milanez, Natural convection in rectangular enclosures heat from below and symmetrically cooled from the sides, Int. J. Heat Mass Transfer 38 (1995) 1063–1073.

[4] A. Lemembre, J.-P. Petit, Laminar natural convection in a laterally heated and upper cooled vertical cylindrical enclosure, Int. J. Heat Mass Transfer 41 (1998) 2437–2454.

[5] O. Agdin, A. Unal, T. Aghan, Natural convection in rectangular enclosures heated from one side and cooled from the ceiling, Int. J. Heat Mass Transfer 42 (1999) 2345–2355.

[6] D. Poulikakos, Natural convection in a confined fluid-filled space driven by a single vertical wall with warm and cold regions, ASME J. Heat Transfer 107 (1987) 867–876.

[7] M. November, M.W. Nansteel, Natural convection in rectangular enclosures heated from below and cooled along one side, Int. J. Heat Mass Transfer 30 (1987) 2433–2440.

[8] I. Sezai, A.A. Mohamad, Natural convection from a discrete heat source on the bottom of a horizontal enclosure, Int. J. Heat Mass Transfer 43 (2000) 2257–2266.

[9] T.S. Chang, Y.L. Tsay, Natural convection heat transfer in an enclosure with a heated backward step, Int. J. Heat Mass Transfer 44 (2001) 2963–2971.

[10] R.L. Frederick, F. Quiroz, On the transition from conduction to convection regime in a cubical enclosure with a partially heated wall, Int. J. Heat Mass Transfer 44 (2001) 1699–1709.

[11] S.K.W. Tou, C.P. Tso, X. Zhang, 3-D Numerical analysis of natural convective liquid cooling of a 3×3 heater array in rectangular enclosures, Int. J. Heat Mass Transfer 42 (1999) 3231–3244.

[12] M.Y. Ha, M.J. Jung, A numerical study on three-dimensional conjugate heat transfer of natural convection in a differentially heated cubic enclosure with a heat-generating cubic conducting body, Int. J. Heat Mass Transfer 43 (2000) 4229–4248.

[13] Y.S. Sun, A.F. Emery, Effects of wall conduction, internal heat sources and an internal baffle on natural convection heat transfer in a rectangular enclosure, Int. J. Heat Mass Transfer 40 (1997) 915–929.

[14] D. Misra, A. Sarkar, Finite element analysis of conjugate natural convection in a square enclosure with a conducting vertical wall, Comput. Meth. Appl. Mech. Eng. 141 (1997) 205–219.

[15] A. Liaqat, A.C. Baytas, Conjugate natural convection in a square enclosure containing volumetric sources, Int. J. Heat Mass Transfer 44 (2001) 3273–3280.

[16] D.-H. Deng, G.-F. Tang, Numerical visualization of mass and heat transport for conjugate natural convection/heat conduction by streamline and heatline, Int. J. Heat Mass Transfer 45 (11) (2002) 2373–2385.

[17] D.-H. Deng, G.-F. Tang, Numerical visualization of mass and heat transport for mixed convective heat transfer by streamline and heatline, Int. J. Heat Mass Transfer 45 (11) (2002) 2387–2396.

[18] S.V. Patankar, Numerical Heat Transfer and Fluid Flow, Hemisphere, Washington, DC, 1980.

[19] T. Hayase, J.A.C. Humphrey, R. Greif, A consistently formulated QUICK scheme for fast and stable convergence using finite-volume iterative calculation procedures, J. Comput. Phys. 98 (1992) 108–118.

[20] De Vahl Davis, Natural convection of air in a square cavity: a benchmark numerical solution, Int. J. Numer. Meth. Fluids 3 (1983) 249–264.

[21] S. Ostrach, C. Raghavan, Effect of stabilizing thermal gradients on natural convection in rectangular enclosures, ASME J. Heat Transfer 101 (1979) 238–243.